WATER TRANSPARENCY IN A BRAZILIAN RESERVOIR

Victor Pedroso Curtarelli[1], Edson Filisbino Freire da Silva[1], Felipe de Lucia Lobo[1], Claudio Clemente Faria Barbosa[1], Evlyn Márcia Leão de Moraes Novo[1]

[1]National Institute for Space Research - INPE, 515, 12227-010, São José dos Campos, Brazil,
victor.curtarelli@gmail.com, edson.freirefs@gmail.com

ABSTRACT

Water transparency is regularly monitored in water reservoirs due to its known relationship with phytoplankton biomass and algal blooms. Transparency is also related to other processes in the watershed, such as the input of suspended particles and dissolved organic matter from overland flow. Therefore, the objective of this study was to map water transparency of a Brazilian reservoir (Paraibuna) after a period of intense rain. In regard of that, water transparency was measured in Secchi depth (Z_{sd}). Then, the relationship between Sentinel-2B MSI bands and Z_{sd} measured in situ were assessed, retrieving empirical models and applying them to the imagery. Results showed that remote sensing reflectance (R_{rs}) increased as Z_{sd} reduced. Z_{sd} was lower in the central area of the reservoir than the periphery areas due to anthropization.

Keywords — water reservoir; Secchi depth; Paraibuna; Paraitinga.

1. INTRODUCTION

Transparency of water is a limnological parameter related to water quality, being monitored in reservoir due to its relationship with the phytoplankton biomass [1] and as an indicator of aquatic system health [2]. In the Funil reservoir, for instance, low transparency has been linked to the occurrence of *M. aeruginosa* bloom [3] while regions of low transparency were related to increase in phytoplankton biomass in the Three Gorges Reservoir [4]. However, changes in phytoplankton biomass is not the only optically active constituent (OAC) affecting water transparency [5].

The most significant OACs in continental aquatic systems are photosynthetic pigments (chl-a), colored dissolved organic matter (CDOM) and total of suspended solids (TSS). Chl-a is a pigment molecule in phytoplankton cells responsible for absorbing the electromagnetic radiation needed for the photosynthesis. CDOM is the fraction of dissolved organic matter, which absorbs electromagnetic radiation of the solar spectrum range of wavelength [6]. TSS can be organic (i.e., phytoplankton) and inorganic (i.e., Feldspar) particles suspended in the water column [7]. Therefore, algae pigments, CDOM and TSS, affect Water transparency of water.

Because of the importance of Water transparency in reservoirs, the objective of this study was to map water transparency in the Paraibuna reservoir after a rainfall event.

2. MATERIAL AND METHODS

2.1 Study Area

This study was conducted in the Paraibuna reservoir (Figure 1), located in São Paulo State, Brazil. Sampling and measurements were performed along 18 stations in the reservoir in August, 8th 2018, from 10:00 to 15:00 (local time). According to the São Paulo Energy Company [8], the water surface of Paraibuna reservoir is 177 km² connected with 47 km² of the Paraitinga river totalizing a 224 km² single system, in a 4150 km² of the watershed. The dams are located at the western margin of the Paraitinga River basin. Paraibuna reservoir is a deep-water reservoir, reaching almost 100 m of depth areas along the former river valleys and values as large as 8 m in the margins.

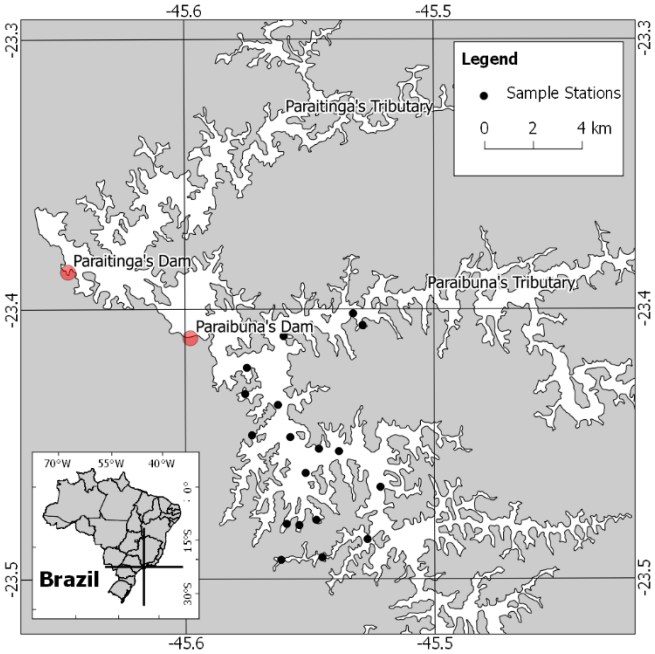

Figure 1. Study area (Paraibuna reservoir) and localization of sampling stations.

Data collection was carried out during an unusual rainfall precipitation that ended a few days before the campaign. Data

from the meteorological station located downstream UHE Paraibuna [6] indicated precipitation not only higher for the winter season (50 mm per month) but much more persistent lasting from July 27th to August 6th of 2018, that is to say, just two days before the campaign (August 8th).

2.2. In Situ Measurements

Secchi depth (Z_{sd}) and remote sensing reflectance (R_{rs}) were measured at 18 sampling stations, while the remaining variables were measured in only 9 stations; TSS concentration in mgL^{-1}, absorption of CDOM at 300 nm in m^{-1}, chlorophyll a (chl-a) in μgL^{-1}. All measurements were conducted at depths deeper than 10 m, avoiding bottom influence in the radiometric measurements.

Z_{sd} is proportional to the sum of the beam attenuation and vertical attenuation coefficients [10]; thus, this study used Z_{sd} as an estimative of water transparency. The same person made all Z_{sd} measurements, lowering the Secchi disk at the sunny side of the boat. For TSS determination, two sampling bottles of water (1.5l) were collected at each sampling station, cooled, and analyzed according to Wetzel and Likens method [11]. Absorption of CDOM was determined according Pegau et al. method [12] using the water filtered previously for TSS determination. Due to the low CDOM absorption, it was measured at 300 nm, since at longer wavelengths the absorption spectra were too noisy. Chl-a was estimated by collecting one sampling bottle (1.5l) of water at each station, which was then cooled, for concentration determination in laboratory according to Wetzel and Likens method [11].

R_{rs} in situ were obtained using a HandHeld 2 VNIR according to Mobley method [13] to correct the glint for the measured data. First, we measured electromagnetic radiation in radiance ($Wm^{-2}sr^{-1}$) onto a pre-calibrated Spectralon plaque (L_p), onto the water surface (L_u), and aiming to the sky (L_s). Then, we calculated R_{rs} by the following equation:

$$R_{rs}(\lambda) = (L_t(\lambda) - pL_s(\lambda)) \ / L_p(\lambda)$$

Where p is the proportion of L_s reflected in the water-atmosphere interface, which must be removed. This parameter was obtained using the rho table of 2015 available on < http://www.oceanopticsbook.info/>.

2.3 Mapping Water Transparency

For mapping water transparency, first, we developed empirical models (ordinary least squared method) between Z_{sd} and simulated bands in R_{rs} of Sentinel-2B MSI sensor the bands employed were B2 (492.1 nm), B3 (559 nm), B4 (664.9 nm), and B5 (703.8 nm). Both, coefficient of determination (R^2) and mean absolute percent error (MAPE) were used as criteria for selecting the best model.

The best model was then applied to the atmospherically corrected Sentinel-2B image acquired in August,11th 2018. Atmospheric correction was carried out using 6S radiative transfer model [14] using a specific script in Python (AtmosPy), provided by the Instrumentation Laboratory of Aquatic Systems (LabISA) in the Brazilian National Institute for Space Research (INPE). The image was provided by the United States Geological Survey (USGS), at the Earth Explorer platform (https://earthexplorer.usgs.gov/).

3. RESULTS

From 18 sample sites, Z_{sd} varied from 1.4 to 2.9 m; chl-a from 1.8 to 9.2 ugL^{-1}; CDOM absorption from 3.6 to 4.5 m^{-1}; and TSS from 1.6 to 3.2 mgL^{-1}.

For all dataset, the highest R_{rs} occurred from 550 to 600 nm, and lowest R_{rs} occurred above 730 nm (Figure 2). Comparing the R_{rs} spectra with the minimum, median and maximum of Z_{sd}, an inverse relationship was noticed, where highest R_{rs} occurred in low Z_{sd}. The inverse relationship indicated backscattering had more contribution than absorption to light attenuation. Backscattering from TSS could reduce the light penetration and increase R_{rs}. In an absorption predominance, R_{rs} should reduce along with Z_{sd}.

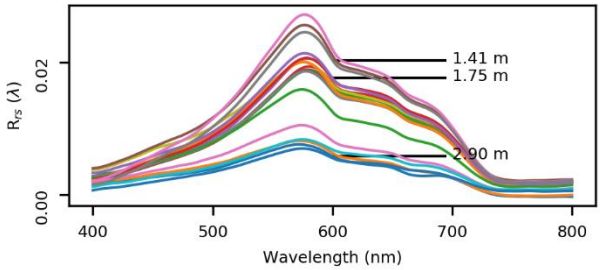

Figure 2. R_{rs} spectra of the 18 sampling stations and its relationship with the minimum, median, and maximum Z_{sd}.

Empirical models were established between all simulated band and the Z_{sd}. All bands showed satisfactory results, with band B4 slightly better (Figure 3).

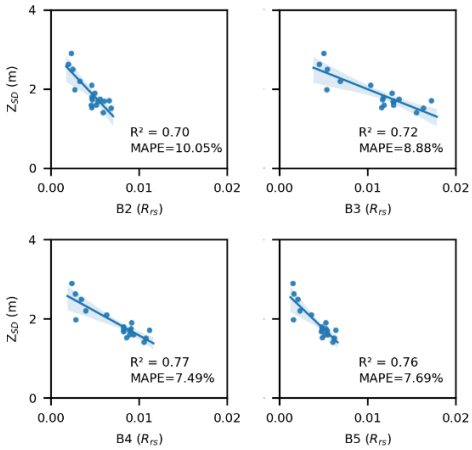

Figure 3. The linear regression relationship between Sentinel-2B MSI simulated bands and Z_{sd}.

We compared all in situ simulated bands with the bands from the image, assessing the atmospheric correction performance. All satellite bands overestimate R_{rs} in situ (Figure 4), probably, due to sun glint in the water-air interface. Near-infrared band $R_{rs,}$ B8 (842 nm), was subtracted from the R_{rs} of visible bands (B2, B3, B4, and B5), to overcome this effect. This procedure can be performed in low TSS concentrations to remove the sun glint [15], which our study showed a maximum of 3.6 mgL^{-1} . Better results (MAPE < 27%) were achieved for bands B4 and B5, although, bands B2 and B3 still overestimate the R_{rs}.

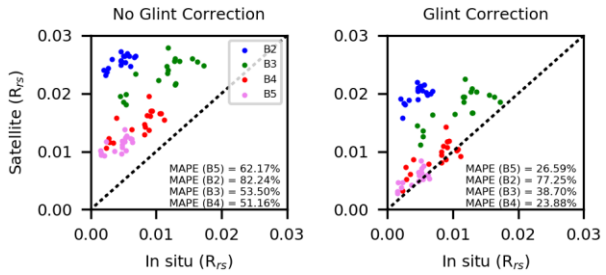

Figure 4. Comparison of Sentinel-2B MSI in situ measured data simulated bands and the image bands from, before and after glint correction.

Band B4 had a good agreement with Z_{sd} (R^2 = 0.77; MAPE = 7.49%) and a satisfactory atmospheric correction (MAPE = 23.88%); thus, we applied this model to the Sentinel-2B MSI image, mapping Z_{sd} in all Paraibuna reservoir (Figure 5).

Estimated Z_{sd} in the central portion of the reservoir (at least 0.5 m) was lower than in the south, where there are narrower branches, and north portions with contributions of Paraitinga and Paraibuna rivers (reaching up to 2.5 m). Due to the rain event on the previous days, the surface runoff generated could carry sediments into the reservoir increasing the TSS in the water column. Besides that, the land use and land cover can affect the sediment contribution into the reservoir during a rain event. To assess the use and land cover we used a pseudo color (R8G4B3) composite with the bands used in this study. The central portion the reservoir margins have a more exposed soil and larger deforested area compared to the north and south margins, where the Z_{sd} was higher. This differences in land cover might explain those differences in water transparency.

The incoming water from the reservoir tributaries in the days after the end of the rain event is composed of clear water from precambrian terrains. Moreover, the high Z_{sd} from this tributaries and branches favors primary productivity indicate by higher chlorophyll-a concentrations, and consequently larger phytoplankton biomass. Whereas, the lower Z_{sd} in the inner reservoir tends to limit phytoplankton productivity, causing smaller chl-a and phytoplankton biomass.

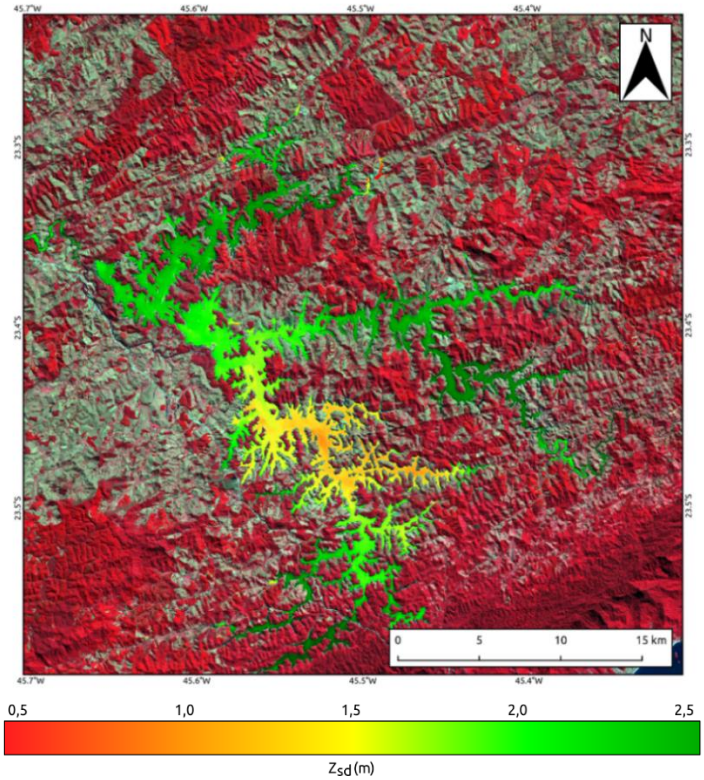

Figure 5. Z_{sd} (Secchi Depth) mapped using the model proposed. Land area Sentinel-2B MSI pseudo color composition (R8G4B3), where the red areas highlights the vegetation and light blue areas highlights anthropization .

4. CONCLUSIONS

The Z_{sd} in the reservoir was mapped after a raining event in the drought period of the year. The central area of the reservoir showed low Z_{sd} than the south and north portions, that showed high Z_{sd}. The sun glint correction achieved better statistics results (as decreased the MAPE for all bands), but B2 and B3 still overestimate the R_{rs} after the correction.

The results suggest that reservoir compartments characterized by low Z_{sd} (central portion) were near margins with large areas of bare soil with little or none vegetation cover, subjected to intense surface runoff generated by the persistent rain, carrying large amount of sediments into the reservoir. Furthermore, bottom influence may be discarded, since sampling points depth are larger than 10 m.

Moreover, a better understanding of the hydrological processes involved in the watershed, land use and land cover leads to better understanding on how the surface runoff influences the sediment carriage into the reservoir. This is a next essential effort, which will help to test the hypothesis raised regarding the central portion of the reservoir relating low Z_{sd} to high sediments contribution derived from increased runoff from reservoir margins characterized by low vegetation cover.

5. AKNOWLEDGEMENTS

This study was financed in part by the Conselho Nacional de Desenvolvimento Científico e Tecnológico (CNPq).

6. REFERENCES

[1] TILZER, M. M. Secchi Disk – Chlorophyll relationships in a lake with highly variable phytoplankton biomass. Hydrobiologia, v. 162, n. 2, pp. 163-171, May 1988

[2] BINDING, C. E.; GREENBERG, T. A.; WATSON, S. B.; RASTIN, S.; GOULD, J. Long term water clarity changes in North America's Great Lakes from multi-sensor satellite observations. Limnology and Oceanography, ASLO, v. 60, p. 1976-1995, 2015.

[3] BRANCO, C. W. C.; ROCHA, M. I. A.; PINTO, G. F. S.; GÔMARA, G. A.; DE FILIPPO, R. Limnological features of Funil Reservoir (R.J., Brazil) and indicator properties of rotifers and cladocerans of the zooplankton community. Lakes and Reservoir: Research and Management, v. 7, n. 2, p. 87–92, 2002.

[4] YANG, Z.; XU, P.; LIU, D.; et al. Hydrodynamic mechanisms underlying periodic algal blooms in the tributary bay of a subtropical reservoir. Ecological Engineering, v. 120, n. 28, p. 6–13, 2018.

[5] BILOTTA, G. S.; BRAZIER, R. E. Understanding the influence of suspended solids on water quality and aquatic biota. ELSEVIER. Water Research. v. 42, p. 2849-2861, June 2008.

[6] LIBES, S. Introduction to Marine Biogeochemistry, Second Edition. 2009.

[7] MOUW, C. B.; GREB, S.; AURIN, D.; et al. Aquatic color radiometry remote sensing of coastal and inland waters: Challenges and recommendations for future satellite missions. Remote Sensing of Environment, 1. abr. 2015

[8] CESP. Usina Hidrelétrica de Paraibuna. Companhia Energética de São Paulo. 2009. Disponível em: <http://www.cesp.com.br/portalCesp/portal.nsf/V03.02/Empresa_UsinaParaibuna?OpenDocument/>

[9] <http://www.snirh.gov.br/hidroweb

[10] KIRK, J. T. O. Light and photosynthesis in aquatic ecosystems. 2nd edition. 1994.

[11] WETZEL, R. G. Limnology - Lake and River Ecosystems, 3rd ed. Academic Press, California. 2001

[12] PEGAU, S.; ZANEVELD, J. R. V; MITCHELL, B. G.; et al. Ocean optics protocols for satellite ocean color sensor validation, Revision 4, Volume IV: Inherent optical properties: instruments, characterizations, field measurements and data analysis protocols. Ocean Color web page, v. IV, n. May, p. 76, 2002.

[13] MOBLEY, C. D. Estimation of the remote-sensing reflectance from above-surface measurements. Applied optics, v. 38, n. 36, p. 7442–7455, 1999.

[14] VERMOTE, E. F.; TANRÉ, D.; DEUZÉ, J. L.; HERMANN, M.; MORCRETTE, J. Second simulation os the satellite signal in the solar spectrum, 6S: an overview. IEEE Transactions on Geoscience and Remote Sensing, v. 35, n. 3, may, 1997.

[15] WANG, M.; SHI, W. The NIR-SWIR combined atmospheric correction approach for MODIS ocean color data processing Menghua. Journal of Geophysical Research, v. 110, n. D10, p. D10S06, 2007